

“Alfvén Profile in the Lower Corona: Implications for Shock Formation”

Running Header: “Alfvén Profile in the Lower Corona”

R. M. Evans¹ and M. Opher²

George Mason University, 4400 University Drive, MSN 3F3, Fairfax, VA 22030

and

W. B. Manchester, IV³ and T. I. Gombosi⁴

Center for Space Environment Modeling, University of Michigan, 2455 Hayward Street, Ann Arbor,
MI 48109

¹ revansa@gmu.edu

² mopher@physics.gmu.edu

³ chipm@umich.edu

⁴ tamas@umich.edu

ABSTRACT

Observations of type II radio bursts and energetic electron events indicate that shocks can form at 1-3 solar radii and are responsible for the GeV/nucleon energies observed in ground level Solar Energetic Particle (SEP) events. Here we provide the first study of the lower corona produced from ten state-of-the-art models. In particular we look to the Alfvén speed profiles as the criteria for shock formation, independent of exciting agent (e.g. flares and CMEs). Global MHD models produce Alfvén speed profiles which are in conflict with observations: a) multiple SEP events are observed with a single exciting agent, but most profiles are missing the “hump” required to form multiple shocks; b) few slow CMEs cause large SEP events, but most profiles drop very quickly, allowing all slow CMEs to drive strong shocks to form between 1-3Rs. Simplified Alfvén wave-driven wind models have steeper profiles but are still in disagreement with multiple shock formation. Only studies that include Alfvén waves with physically based damping are in agreement with observations. This implies the results of these 1D local studies must be included in global models before we can study shock formation in the lower corona.

SUBJECT HEADINGS: MHD – Sun: corona – Sun: magnetic fields – Sun: coronal mass ejections (CMEs) – solar wind – shock waves

1. INTRODUCTION

Recent studies of type II radio bursts and energetic electron events (Reiner & Kaiser 1999; Klassen et al. 2002; Classen & Aurass 2002; Mewaldt et al. 2003) indicate that Coronal Mass Ejection (CME)-driven shocks can form and accelerate particles very low in the corona. Tylka et al. 2003 found that the very high energy (GeV/nucleon) Solar Energetic Particles (SEPs) observed in ground level events are accelerated by CME-driven shocks at 1-3Rs (solar radii). In a type II radio burst survey Gopalswamy et al. 2005 determined an average source CME height of 1.6-2.2Rs. Gopalswamy et al. 2005 also found only five of 72 sampled CMEs that were the source of a large SEP event had $v < 1,000$ km/s.

Type II radio bursts and energetic electron events also have found that flares or other sources drive shocks in the lower corona which accelerate high energy SEPs (Gopalswamy et al. 1998; Cane & Erickson 2005; Mann, Aurass & Warmuth 2006; Kahler 2007). A shock forms when a subsonic object drives a pressure wave that steepens into a shock, or when a disturbance traveling slower (or faster) than the background Alfvén speed forms a slow-mode (or fast-mode) shock. Here we focus on fast-mode shocks because of their strength and ability to accelerate high energy SEPs. In the rest frame of the solar wind, a fast-mode shock will form if the exciting agent travels faster than the background Alfvén speed. This paper focuses on shocks independent of the exciting agents. Shocks are “a discontinuity well-defined in magnetohydrodynamics and, consequently, independent of the exciting agent.” (Forbes et al. 2006)

Multiple shock formation is also motivated by type II radio bursts and energetic electron events, as were observed with the CME event on 1997 May 12. It produced two shock waves, one in the corona and one in interplanetary space (Gopalswamy & Kaiser 2002). Shanmugaraju et al. 2005 completed a study of 38 instances of two SEP events occurring within 30 minutes of each other and found that most (90%) were associated with both a CME and a flare, and that none were associated with multiple CMEs or multiple flares, indicating that some of these multiple SEP events have one single CME or a single flare as the source. Whether the potential exciting agent (flare or CME) forms no shock, one shock, or multiple shocks in the lower corona depends on the profile of the Alfvén speed (and the magnetosonic speed) (Forbes et al. 2006). Here we review the current state-of-the-art models and relate the implications of the method of driving the solar wind on the lower corona, in particular in the Alfvén speed profile.

Our knowledge of the solar wind background and Alfvén speed in the lower corona stems from semi-analytic models (e.g. Mann et al 2003, Sittler & Guhathakurta 1999) that use electron number density observations as constraints, and 3D global MHD models that use observed photospheric magnetic field. Current methods for driving the solar wind in MHD models include empirical heating functions, varied polytropic index and the inclusion of Alfvén wave pressure and momentum (e.g. Mikic et al. 1999; Gombosi et al. 2000; Groth et al. 2000; Usmanov et al. 2000; Riley et al. 2001; Manchester et al. 2004b; Toth et al. 2005; Usmanov & Goldstein 2006). From these models we learned about the interaction of CMEs with the background solar wind, such as the angular extent of the CME-driven shock front and the variation of Mach number with latitude (Manchester et al. 2005).

In this paper we examine the Alfvén profiles from ten models, six global MHD: Manchester et al. 2004a, b (herein MA04); Cohen et al. 2007 (herein CO07); Roussev et al. 2004 (herein RO04); Riley 2006 (herein RIL06); Lionello, Linker & Mikic 2008 (herein LI08); Usmanov & Goldstein 2006 (herein UG06); and two local studies: Cranmer, van Ballegoijen & Edgar 2007 (herein CR07); Verdini & Velli 2007 (herein VE07) and two semi-analytic models: Guhathakurta, Sittler & Ofman 2006 (herein GSO06); and Mann et al. 2003 (herein MAN03). All models are chosen for solar minima conditions and all are able to reproduce solar wind conditions near Earth.

A major challenge in MHD modeling is driving the solar wind. Observations have shown that the solar wind consists of two parts: a slow wind originating from regions of closed field lines, and a fast wind originating from regions of open field lines. It is well known that some sort of momentum in addition to thermal pressure must be added in order to drive the solar wind, although there is not yet a cohesive approach to the problem. If one uses ideal MHD without some sort of additional momentum, the ratio of the density at 1 AU to the coronal density is too high. As a result, when one matches the density at either the inner boundary or at 1AU to observations, the density at the other boundary will be highly inaccurate (see discussion in Usmanov & Goldstein 2003). To solve this problem and produce a fast wind of relatively low density while preserving agreement with the plasma density observed at the coronal base, an additional source of momentum must be incorporated into the models (Munro & Jackson 1977; Barnes et al. 1995).

Among the numerous possible sources of additional solar wind acceleration, Alfvén waves are one of the most attractive. The ability of the waves to produce an additional nonthermal acceleration and to bring models into agreement with observations both near the Sun and at large distances was recognized more than three decades ago. The fast and slow magnetosonic modes are not good candidates because they are damped close to the Sun and therefore unable to provide the momentum over distances of a few solar radii, as is required to match observations.

The development of precise global MHD models is crucial because the 3D structure of the corona determines both the eruptive activities and the background in which they propagate. Understanding this environment is imperative for real time space weather forecasting. The inclusion of 3D magnetogram data for active regions in global models will provide improved modeling capabilities. Current magnetograms incorporated into MHD models (Roussev et al. 2004, Cohen et al. 2007, Lionello, Linker & Mikic 2008) are generated from line-of-sight measurements (Arge & Pizzo 2000).

A present difficulty facing global MHD models is that they are limited by the difficulty of treating microphysics over large scales, for example resolving the several orders of magnitude variations of density and temperature across the transition region. As a result, most MHD models start at the base of the lower corona and extrapolate the field from the photosphere, and make use of approximations. Local models are useful because they include higher resolution, and can more accurately treat physical processes and model the photosphere, chromosphere and transition region individually.

Local studies have been used to examine the unresolved issue of preferential ion heating in coronal holes, which was observed by SOHO's Ultraviolet Coronagraph Spectrometer and also

predicted by the first ion cyclotron resonance studies from two decades ago (e.g. Hollweg 1986, Hollweg & Johnson 1988, Isenburg 1990; see discussion in Hollweg 2006). The difficulty is to explain how the energy gets into the high frequency waves: on small scales, the energy is known to be in lower frequencies (Howes 2006). Among the possible mechanisms for transferring the energy to the high frequencies - the sources of coronal heating - are reconnection (e.g., Matthaeus et al. 2003), heat flux driven plasma instabilities (e.g. Markovskii et al. 2006) and MHD turbulence (e.g. Matthaeus et al. 1999, Chandran 2005). Rappazzo et al. (2007) performed high resolution simulations of MHD turbulence in a coronal loop described by reduced MHD equations. A result of this study was that the heating rate scaled with the intensity of the magnetic field, varying as $B^{3/2}$ for weak fields and B^2 for strong fields. The goal for global MHD models is to incorporate what has been learned in local heating studies to obtain a realistic background solar wind in the lower corona.

The paper is organized as follows: Section 2 describes the models; Section 3 describes the Alfvén speed profile obtained for each model; and Section 4 provides Discussion and Conclusions.

2 MODELS

Below we describe the ten models whose Alfvén speed we analyzed in the lower corona. The first group of models (Section 2.1) is global MHD models which drive the solar wind with thermal heating functions; the second group (Section 2.2) is semi-analytic models, and the final group (Section 2.3) is MHD models which include damped Alfvén waves. The magnetic fields are modeled as multipole expansions or calculated from the Potential Field Source Surface (PFSS) model using magnetograms. The density is either constrained by observations or solved using MHD equations and an assumed density at the inner boundary. See Table 1 for an overview of aspects of each model (labeled M1-M10). All models were chosen for solar minima conditions.

2.1 3D Global MHD Models with Thermal Empirical Heating: M1-M5

2.1.1 M1: Manchester et al. 2004 (MA04)

Groth et al. 2000 introduced an empirical heating function (exponentially decreasing and latitude dependent) into the MHD equations to drive the solar wind by recreating the effects of energy absorption, thermal conduction and radiative losses. This steady-state solar wind model was used in MA04 to model the propagation of a CME from the Sun to 1 AU. The magnetic field is treated as a multipole expansion using observations as constraints. The advantages of this model are that it provides a global 3D picture and agreement with observations near 1AU. The disadvantages of this model are that it uses a simplified magnetic field model and drives the solar wind solely with thermal heating.

2.1.2 M3: Roussev et al. 2004 (RO04)

RO04 extended the model of Groth et al. 2000 by incorporating magnetograms and using the Potential Field Source Surface (PFSS) model to extrapolate the magnetic field from the photosphere into the corona. The PFSS model has been successful at predicting interplanetary magnetic field polarity and the solar wind speed at Earth (Arge and Pizzo 2000); however it is known that PFSS models obtain a weak magnetic field value at 1 AU. This problem is currently resolved by increasing the magnetic field intensity at the Sun. This model employs a non-uniform polytropic index distribution, as in Roussev et al. 2003. The advantages of this model are that it provides a global 3D picture, agreement with observations near 1AU, and a complex magnetic field configuration. The disadvantage of this model is that it drives the solar wind solely with thermal heating.

2.1.3 M2: Cohen et al. 2007 (CO07)

Like RO04, CO07 includes magnetograms and employs a non-uniform polytropic index distribution to drive the solar wind. The Wang-Sheeley-Arge (WSA) PFSS model is used in conjunction with the Bernoulli integral to solve extrapolate the polytropic index from the source surface to the solar surface along magnetic field lines, resulting in a polytropic index which depends on

solar wind velocity and temperature. The model is tested for both solar minima and maxima conditions, and the solar wind velocities at 1 AU matched better to observations for solar minima conditions. For this study, we include the model with CR1922 (solar minima conditions). The advantages of this model are that it provides a global 3D picture, agreement with observations near 1AU, and a complex magnetic field configuration. The disadvantage of this model is that it drives the solar wind solely with thermal heating.

2.1.4 M4: Riley 2006 (RIL06)

The polytropic 3D MHD model of RIL06 also makes use of magnetograms. RIL06 uses an adiabatic energy equation with a reduced polytropic index and solves the set of resistive MHD equations (Mikic et al. 1999). The model is from a study of the CME eruption of 2005 January 20. The CME originated from AR720 in the northern hemisphere at approximately 180 degrees Carrington longitude. The advantages of this model are that it provides a global 3D picture and a complex magnetic field configuration. The disadvantages of this model are that it produces an unrealistic density profile and drives the solar wind solely with thermal heating.

2.1.5 M5: Lionello, Linker & Mikic 2008 (LI08)

LI08 is a 3D MHD model that differs from the other global MHD models in that the lower boundary extends down to include the chromosphere and transition region (Lionello, Linker & Mikic 2001), while others start in the lower corona. The magnetic field configuration is generated using smoothed magnetograms, and the profiles in this study correspond with CR1913. The model includes uniform viscosity and uniform resistivity, both of which are smaller than realistic values by computational limitations. The model uses an energy equation which explicitly treats radiation loss and coronal heating, and includes a term to represent (undamped) Alfvén waves in the WKB approximation. The coronal heating is decomposed into empirical quiet sun heating and active region heating terms, both dependent on the magnetic field. Additionally, an empirical exponential function similar in form to that of MA04 except that it depends only on radial distance is applied everywhere. The advantages of this model are that it utilizes magnetograms, it includes the chromosphere and transition region and an improved energy equation including Alfvén wave momentum. The disadvantage of this model is that it primarily drives the solar wind with thermal heating.

2.2 Semi-analytic Models: M6 & M7

2.2.1 M6: Mann et al. 2003 (MA03)

MAN03 is a semi-empirical model for an equatorial active region. The magnetic field is a background quiet Sun (which goes like $1/r^2$) superimposed with an active region modeled as a dipole. The electron density is a combination of two models: starting at the solar surface, a one-fold Newkirk (1961) model is used until 1.8Rs, where the solution is matched with the model from Mann et al. 1999, which matches well with Wind observations above 1.8 Rs and is suitable for active regions. The reason for the two sources is because the Newkirk model matches better to observations in the quiet equatorial region near the Sun, but fails to match above 1.8 Rs. The advantage of this model is that it utilizes an observed density profile. The disadvantages of this model are that it is a 2D model and it uses a simplified magnetic field model.

2.2.2 M7: Guhathakurta, Sittler & Ofman 2006 (GSO06)

Sittler & Guhathakurta 1999 (herein SG99) developed a global electron density is derived from observations (SOHO Whole Sun Month and Ulysses data, see SG99). The magnetic field in GSO06 is also taken from SG99, and takes the form of a multipole expansion whose expansion factors are constrained by coronal observations (SOHO/EIT and Ulysses). The chosen magnetic field produces good results in the polar regions, but is poorly applicable in the equatorial region. As a result, the Alfvén speed profile for the equator from this model is taken above 2.5Rs. The advantages of this model are that utilizes observed values of density and magnetic field. The disadvantages of this model are that it is a 2D model and it drives the solar wind solely with thermal heating.

2.3 Models with Alfvén Wave-Driven Winds: M8, M9 & M10

2.3.1 M8: Cranmer, van Ballegoijen & Edgar 2007 (CR07)

CR07 drives the solar wind with Alfvén waves and MHD turbulence. This 1D radial model contains acoustic and Alfvén wave pressure to accelerate the solar wind, utilizing acoustic waves to heat the chromosphere and Alfvén waves in the corona. The main strategy is to cascade the energy from large scale Alfvénic fluctuations to high frequency collisionless kinetic modes. This cascade is accomplished by partially reflecting Alfvén waves to create ingoing waves to damp the outgoing waves. As in Cranmer & van Ballegoijen (2005), the initial magnetic field structure is a multipole expansion slightly modified from Banaszekiewicz et al. (1998)'s model. The initial radial dependence of the electron density is derived to match white-light polarization brightness measurements in the extended corona. Their model includes terms from radiation, conduction, Alfvén and acoustic wave damping. The advantage of this model is that it includes waves and thermal heating. The disadvantages of this model are that it is 1D radial and applies solely to coronal holes.

2.3.2 M10: Verdini & Velli 2007 (VE07)

VE07 is a local heating model including a static photosphere and chromosphere, transition region, and open corona. Global MHD models do not include these lower regions because of the high resolution needed to resolve these layers, instead using the corona as a lower boundary. VE07 incorporate Alfvén wave reflection and dissipation and use Ulysses and Helios data as constraints. The numerical model solves the MHD equations assuming incompressible, adiabatic transverse fluctuations in the velocity and the magnetic field, following waves in the frequency range 10^{-6} Hz to 10^{-2} Hz. The chromosphere and photosphere are considered to be isothermal, with an exponentially varying density and a flux tube geometry chosen to agree with a quiet Sun coronal hole model (Hollweg, Jackson & Galloway 1982). In the corona, the temperature is given by the semi-empirical model of Casalbuni et al. (1999). The advantages of this model are that it drives the solar wind with waves, it includes the lower layers of the solar atmosphere, and it uses observations as constraints. The disadvantages of this model are that it uses a simplified density model and it does not provide a global picture.

2.3.3 M9: Usmanov & Goldstein 2006 (UG06)

In this 3D model, the solar wind is driven by including Alfvén wave momentum and energy in the WKB approximation. WKB approximation is valid as long as the waves have wavelengths shorter than local characteristic scale. WKB approximation is useful in a global model because it does not require a high-resolution description of the momentum and energy transformations from the waves to the flow. The set of MHD equations solved include an additional equation with two new variables: the Alfvén wave energy density and the velocity of the Alfvén waves. The MHD equations are solved only in the inner region (1-20Rs), and in the outer region the solution is given by forward integration along the hyperbolic radial coordinate. The free parameters were chosen to fit the Ulysses data and the computed values match fairly well near 1 AU. The advantages of this model are that it provides a global 3D picture and it drives the wind with Alfvén wave momentum. The disadvantages of this model are that it uses a simplified magnetic field model and artificial damping for Alfvén waves.

3. PROFILES

Figure 1 shows the Alfvén speed profiles for all models: polar/open field region profiles are in Figure 1a, equatorial streamer profiles in Figure 1b, and active region profiles in Figure 1c. Tables 2-4 provide locations of features of the models. In Figure 2, we show a contour plot of Alfvén speed for CO07, and indicate where the line plots were taken for each model.

For the semi-analytic models (M6 and M7), there are two characteristics of the Alfvén speed profiles: a valley around 1.5Rs (solar radii) in MAN03, and a hump around 3.8Rs in both MAN03 and GSO06 (see Figures 1b and c). These profiles are consistent with the studies of type II radio bursts mentioned earlier that indicate shocks can form at 1-3 Rs. Also, the valley and hump structures allow

for the formation of multiple shocks. Although simplified models, the semi-analytic studies are based on observed values of density and magnetic field. For the MAN03 profile, a driving agent (e.g. CME or flare) with velocity $500\text{ km/s} < v < 800\text{ km/s}$ could form a shock between 1-3Rs. The shock would dissipate by 4Rs as a result of the hump in the Alfvén speed, and reform after 5Rs.

For the global MHD models driving the solar wind with thermal heating (M1, M2, M3, M4, M5), the profile in the equatorial region either: drops off quickly to $<500\text{ km/s}$ below 1.4Rs; or has a hump and a low Alfvén speed ($<500\text{ km/s}$) in the lower corona. In Figure 1b, M2A and B correspond to variations in thermal heating in the same model. In Figure 1c, the letters C, D and E for M2 indicate the direction of propagation out of the active region: C is straight out through the center; D and E are taken at an angle from the center of the AR, D lies in a meridional plane and E in a plane parallel to the equatorial plane.

For the global MHD model with Alfvén wave-driven wind and unrealistic damping (M9), the profile falls off much less rapidly than the MHD models that use empirical heating (see Figure 1b). However, by 5Rs it matches well with the other global MHD profiles. This profile does not contain a hump.

For the local studies of Alfvén wave-driven winds (M8 and M10), the profiles contain a hump, although very close to the Sun, below 2Rs (see Figure 1a). Below 8Rs, the magnitude of the Alfvén speed for these two models is larger than the global MHD models that only include thermal heating, and smaller than for the semi-empirical model. Also, the hump is closer to the sun for the models including Alfvén waves compared to the semi-empirical model.

In the plots shown in Figure 1, the Alfvén speed profile for streamers was taken from the line through the center of the streamer (see Figure 2). We investigated the effect of the direction of propagation on the Alfvén profile using one single MHD model (see Figure 3). The motivation was that a) the Alfvén speed will have directional dependence as $B\cos\theta$ and b) the MAN03 plot of Alfvén speed (which shows a clear hump) is taken 45 degrees away from the line through the center of the active region. We took new profiles from 45 degrees away from the streamer for the CO07 model with three variations (labeled a, b and c in Figure 3) in thermal heating obtained by varying the magnetic field (in order of increasing strength, a, c, b) and density (in order of increasing value a, c, b) at the inner boundary (solar surface).

In the quiet sun, propagation at an angle has two effects: a hump develops around 5-6 Rs for all three cases of variation of thermal heating. For propagation straight out of the streamer, the Alfvén speed drops quickly for all three cases. Finally, we investigated the Alfvén speed profile near an active region. The Alfvén speed profile was found to be comparable to the fast polar profile 0.2Rs above the surface and enhanced compared to the quiet sun until 0.5 Rs for model M2. In model M4, a profile taken 10 degrees Carrington latitude away from an AR still differed from the quiet sun profile. Also, profiles which were taken at angle out of an AR were found to differ in magnitude and location of hump (see Tables 3 and 4) from each other and from the profile taken straight out of the AR.

4. DISCUSSION AND CONCLUSIONS

In the present paper we for the first time look in details on the implication of the method of driving the solar wind on the lower corona, in particular in the Alfvén speed profile.

State-of-the-art global MHD modeling has allowed for numerous studies of the formation, propagation, and interaction of solar phenomena such as CMEs with the Earth's magnetosphere. This modeling is a powerful tool to create a realistic 3D picture of these solar disturbances. Most models are benchmarked with plasma parameters near 1 AU from observations of satellites such as ACE, Wind, Ulysses and STEREO. Although the MHD models consistently reproduce aspects such as density and magnetic field structure, and the bimodality of the solar wind at 1 AU, we have shown here that they

are not consistent with respect to Alfvén speed in the lower corona as a result of the different methods of solar wind acceleration and coronal heating.

We have completed an analysis of state-of-the-art 3D MHD, semi-analytic and local models, in particular the Alfvén speed profile in the lower corona. We related current observations to the different Alfvén speed profiles produced by the models. For the profile at an active region on the Sun (Figure 1c), we found that the environment near an active region from global MHD models with thermal heating functions is one in which a) the profiles drop off too quickly, allowing slow exciting agents to form strong shocks at heights of 3Rs or less; and b) the valley and hump characteristics expected from the semi-analytic models of Mann et al. 2003 and Guhathakurta, Sittler & Ofman 2006 are not reproduced. These results are in contrast to studies of type II radio bursts and energetic electron events: a) strong shocks form low in the corona at 1-3Rs and accelerate high energy SEPs (Tylka et al. 2003); b) multiple shocks and SEP events are observed with a single CME and a single flare source (Gopalswamy & Kaiser 2002, Shanmugaraju et al. 2005); and c) five CMEs with $v < 1,000$ km/s were the source of a major SEP event during solar cycle 23 (Gopalswamy et al. 2005). We emphasize here that shock formation and evolution should be considered independent of the exciting agent (Forbes et al. 2006).

The inclusion of Alfvén waves with unrealistic damping in a global MHD model steepens the Alfvén speed profile, but it is still not in agreement with these observations. Only local studies including Alfvén waves with physically motivated damping achieve: a) the steepened profile and b) the hump needed to align the models correctly with observations from type II radio bursts and energetic electron events. This implies the results of these studies must be included in global models before we can study shock formation in the lower corona.

We also looked in the effect of the direction of propagation of the exciting agent, for example a CME. We found that forming multiple shocks is not only dependent on the driving agent's speed and Alfvén speed, but also on the direction of propagation from the active region. A CME which propagates at an angle to the streamer will be more likely to form multiple shocks.

ACKNOWLEDGEMENTS

This research was partially supported by the LWS NNG06GB53G and National Science Foundation CAREER Grant ATM-0747654. M. O. and R. E. would like to thank Marco Velli, Arcadi Usmanov, Ofer Cohen and Roberto Lionello for their cooperation during this project. R. E. would like to thank Aline Vidotto, Cristiane Loesch and Yong Liu for valuable discussions.

REFERENCES

- Arge, C. N. & Pizzo, V. J. 2000, *J. Geophys. Res.*, 105, 10465
- Banaszkiewicz, M., Axford, W. I. & McKenzie, J. F. 1998, *A&A*, 337, 940
- Barnes, A., Gazis, P. R. & Phillips, J. L. 1995, *Geophys. Res. Lett.*, 22, 3309
- Casalbuoni, S., Del Zanna, L., Habbal, S. R. & Velli, M. 1999, *J. Geophys. Res.*, 104, 9947
- Chandran, B. D. G. 2005, *Phys. Rev. Lett.*, 95, 265004
- Classen, H. T. & Aurass, H. 2002, *A&A*, 384, 1098
- Cohen, O., et al. 2007, *ApJ*, 654, L163
- Cranmer, S. R. & van Ballegooijen, A. A. 2005, *ApJ SS*, 156, 265
- Cranmer, S. R., van Ballegooijen, A. A. & Edgar, R. J. *ApJ SS*, 2007, 171, 520
- Forbes, T. G. et al. 2006, *Space Science Reviews*, 123, 1-3, 251
- Gombosi, T. I., DeZeeuw, D. L., Groth, C. P. T., Powell, K. G. & Stout, Q. F. 2000, *Journal of Atmospheric and Solar-Terrestrial Physics*, 62, 1515
- Gopalswamy, N. et al. 1998, *J. Geophys. Res.*, 103, 307G
- Gopalswamy, N. & Kaiser, M. R. 2002, *Adv. Space Res.*, 29, 307
- Gopalswamy, N., Aguilar-Rodriguez, E., Yashiro, S., Nunes, S., Kaiser, M. L. & Howard, R. A. 2005, *J. Geophys. Res.*, 110, A12S07
- Groth, C. P. T., De Zeeuw, D. L., Gombosi, T. I. & Powell, K. G. 2000, *J. Geophys. Res.*, 105, 25053
- Guhathakurta, M., Sittler, E. C. & Ofman, L. 2006, *J. Geophys. Res.*, 111, A11215
- Hollweg, J. V. 1986, *J. Geophys. Res.*, 91, 4111
- Hollweg, J. V. 2006, *J. Geophys. Res.*, 111, A12106
- Hollweg, J. V., Jackson, S. & Galloway, D. 1982, *Sol. Phys.*, 75, 35
- Hollweg, J.V. & Johnson, W. 1988, *J. Geophys. Res.*, 93, 9547
- Howes, G. G., Cowley, S. C., Dorland, W., Hammett, G. W., Quataert, E. & Schekochihin, A. A. 2006,

ApJ, 651, 590

Kahler, S. W. 2007, Space Sci. Rev., 129, 359

Klassen, A., Bothmer, V., Mann, G., Reiner, M. J., Krucker, S., Vourlidas, A. & Kunow, H. 2002, A&A, 385, 1078

Klein, K. L. & Trotter, G. 2001, Space Sci. Rev., 95, 1, 215

Isenburg, P. A. 1990, J. Geophys. Res., 95, 6437

Lionello, R., Linker, J. A. & Mikic, Z. 2001, ApJ, 546, 542

Lionello, R., Linker, J. A. & Mikic, Z. 2008, submitted ApJ

Markovskii, S. A., Vasquez, B. J., Smith, C. W. & Hollweg, J. V. 2006, ApJ, 639, 1177

Manchester, W. B., Roussev, I., Opher, M., Gombosi, T. I., De Zeeuw, D. L., Toth, G., Sokolov, I., Powell, K. G. 2004a, J. Geophys. Res., 109, A01102

Manchester, W. B., Gombosi, T. I., Roussev, I., Ridley, A., De Zeeuw, D. L., Sokolov, I. V., Powell, K. G. & Tóth, G. 2004b, J. Geophys. Res., 109, A02107

Manchester, W. B., et al. 2005, ApJ, 622, 1225

Mann, G., Jansen, F., MacDowall, R. J., Kaiser, M. L. & Stone, R. G. 1999, A&A, 348, 614

Mann, G., Klassen, A., Aurass, H. & Classen, H.T. 2003, A&A, 400, 329

Mann, G., Aurass, H & Warmuth, A. 2006, A&A, 454, 969

Matthaeus, W. H., Zank, G. P., Oughton, S., Mullan, D. J. & Dmitruk, P. 1999, ApJ, 523, L93

Matthaeus, W. H., Dmitruk, P., Oughton, S. & Mullan, D. 2003, in AIP Conference: Proceedings of the Tenth International Solar Wind Conference., Vol. 679, 427

Mewaldt, R. A. et al. 2003, Proceedings of the 28th International Cosmic Ray Conference. Editors: T. Kajita, Y. Asaoka, A. Kawachi, Y. Matsubara and M. Sasaki, pg. 3313

Mikic, Z., Linker, J. A, Schnack, D. D., Lionello, R. & Tarditi, A. 1999, Phys. Plasmas, 6, 2217

Munro, R. H. & Jackson, B. V. 1977, ApJ, 213, 874

Newkirk, G. Jr. 1961, ApJ, 133, 983

Rappazzo, A. F., Velli, M., Einaudi, G. & Dahlburg, R. B. 2007, ApJ, 657, L47

Reiner, M. J. & Kaiser, M. L. 1999, J. Geophys. Res., 104, A816979

Riley, Linker, & Mikic, Z. 2001, J. Geophys. Res., 106

Riley, J. 2006 SHINE presentation <http://shadow.adnc.net/~pete/research/va-study-cr2025.htm>

Roussev, I. I., et al. 2003, ApJ, 595, L57

Roussev, I. I., Sokolov, I. V., Forbes, T. G., Gombosi, T. I., Lee, M. A. & Sakai, J. I. 2004, ApJ, 605, L73

Shanmugargju, A., Moon, Y. J., Cho, K. S., Kim, Y. H., Dryer, M. & Umapathy, S. 2005, Sol. Phys., 232, 87

Sittler, E. C., Jr. & Guhathakurta, M. 1999, ApJ, 523, 812

St. Cyr, O. C., et al. 2000, J. Geophys. Res., 105, 18169

Tóth, G., et al. 2005, J. Geophys. Res., 110, A12226

Tylka, A. J. et al. 2003, Proceedings of the 28th International Cosmic Ray Conference. Editors: T. Kajita, Y. Asaoka, A. Kawachi, Y. Matsubara and M. Sasaki, pg. 3305

Tylka, A. J., Cohen, C. M. S., Dietrich, W. F., Lee, M. A., Maclellan, C. G., Mewaldt, R. A., Ng, C. K., & Reames, D. V. 2005, ApJ, 625, 474

Usmanov, A.V., Goldstein, M.L., Besser, B.P. & Fritzer, J.M. 2000, J. Geophys. Res., 105, 12675

Usmanov, A. V. & Goldstein, M. L. 2003, J. Geophys. Res., 108(A9), 1354

Usmanov, A. V. & Goldstein, M. L. 2006, J. Geophys. Res., 111, A07101

Verdini, A. & Velli, M. 2007, ApJ, 662, 66

TABLE1: Summary of the key components for each model. The labels match with the legend labels in FIGURE 1, and are given as follows: Manchester et al. 2004a, b (MA04; M1); Cohen et al. 2007 (CO07; M2); Roussev et al. 2004 (RO04; M3); Riley 2006 (RIL06; M4); Lionello, Linker & Mikic 2008 (LI08; M5); Guhathakurta, Sittler & Ofman 2006 (GSO06; M6); Mann et al. 2003 (MAN; M7); Cranmer, van Ballegooijen & Edgar 2007 (CR07; M8); Usmanov & Goldstein 2006 (UG06; M9); and Verdini & Velli 2007 (VE07; M10).

Model	Reference	General Description	Magnetic Field	Density	Driving the Solar Wind	Polytropic Index
M1	MA04	3D Global MHD Model	Multipole Expansion	Computed w/ n_0 at the boundary chosen	Empirical Heating Function (Exponential)	Fixed
M2	CO07		WSA PFSS Model	Bernoulli integral solves γ	Empirical Heating Function (B-dependent)	Varied
M3	RO04			Computed w/ n_0 at the boundary chosen	Empirical Heating Func.	
M4	RIL06				Locally determined Empirical Heating Function (B-dependent)	Fixed
M5	LI08	3D MHD; Treats Transition Region; Includes Wave Momentum	Synoptic Map Input			Fixed
M6	GSO06	Semi-Empirical 2D Global MHD Model	Multipole Expansion	Electron density from observations	Empirical Heating Function (Product of Exp. and $1/r^3$)	Fixed
M7	MAN03	Semi-Empirical Model; Suitable for equatorial active region	Semi-empirical dipole superimposed on $1/r^2$	(Newkirk 1961) & (Mann 1999) models include observations
M8	CR07	1D Radial HD; Suitable for coronal holes	2D Model of open flux tubes (Cranmer 2005) in Multipole Expansion (Banaszkiewicz 1998)	Computed w/ n_0 at the boundary chosen	Empirically guided acoustic waves; Alfvén waves (reflected and damped) with non-WKB	Fixed
M9	UG06	3D Global MHD model	Tilted-dipole		Alfvén wave pressure added in WKB approximation in open field regions	
M10	VE07	1D MHD model; Suitable for coronal holes	Open Flux Tube (Hollweg 1982)	Exponential Density	Turbulent Dissipation using Alfvén Waves	Fixed

TABLES CORRESPONDING TO PLOTS:

Model	X [Rs]	Va [km/s]
M1	1.28	2,200
M2	1.38	2,500
M5	1.41	3,800
M6	1.78	5,400
M8	1.32	3,200
M9	1.00	3,500
M10	1.50	3,100

TABLE 2: Maximum Alfvén speed location and value for the Poles (See FIGURE 1a).

Model	Valley X [Rs]	Valley Va [km/s]	Hump X [Rs]	Hump Va [km/s]
M1	-	-	1.00	1,300
M2A	1.2	400	1.73	660
M2B	2.87	180
M4A	1.53	540
M5	1.70	78	1.08	140
			3.80	350
M6	3.65	820
M9	1.00	1,600

TABLE 3: Main features for Streamers that present a “hump” (See FIGURE 1b). It gives the position of valley and hump structures, and the Alfvén speed.

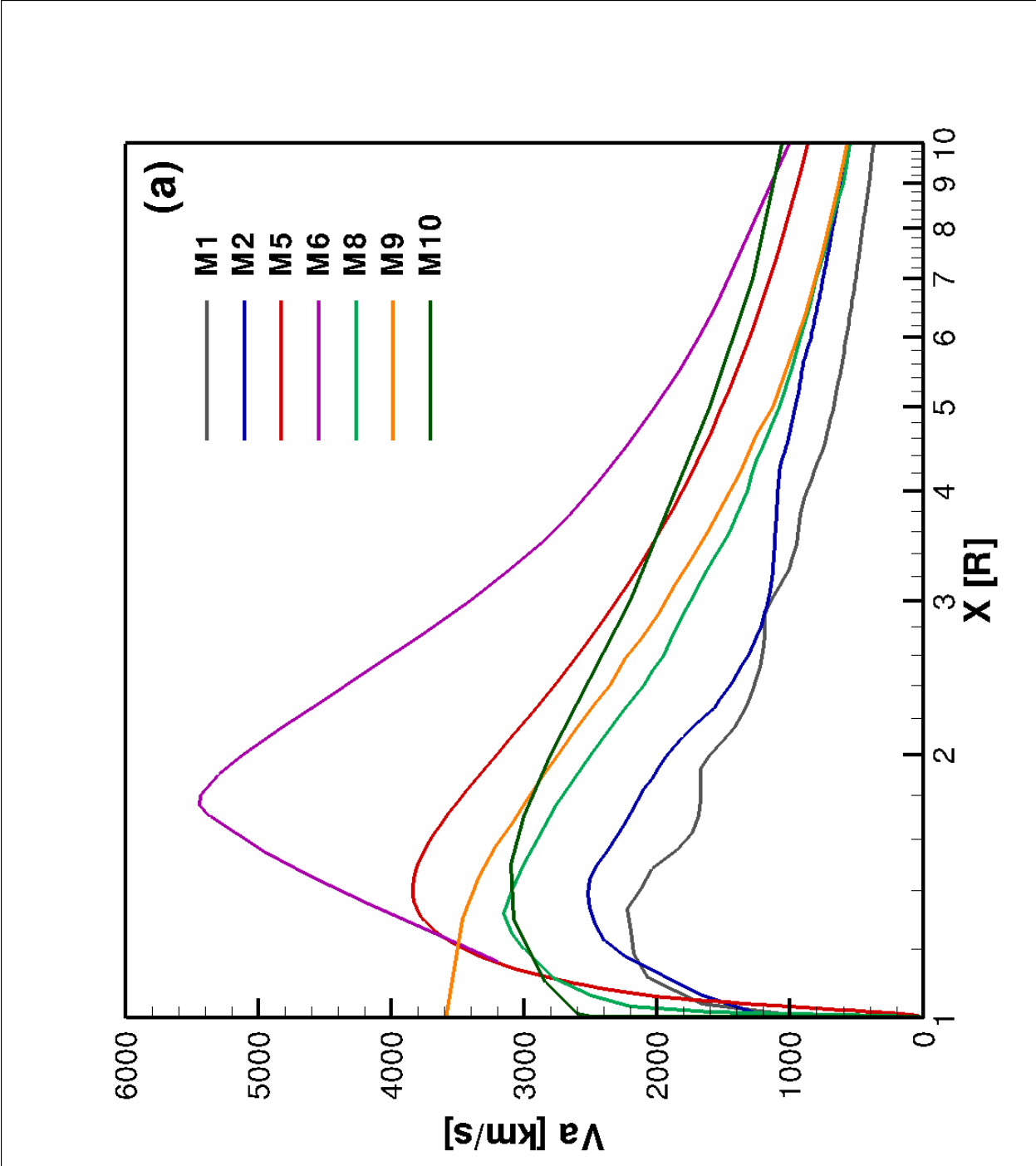
TABLE 4: Same as Table 3, but for Active Regions (See FIGURE 1c).

Model	Valley X [Rs]	Valley Va [km/s]	Hump X [Rs]	Hump Va [km/s]
M2C	3.12	220	7.00	410
M2D	4.00	74	7.75	135
M2E	3.84	110	6.70	215
M3	1.00	7,800
M4B	2.96	85	4.00	100
M4C	2.20	300	3.5	305
M5	1.50	240	1.80	290
M7	1.55	425	3.85	740

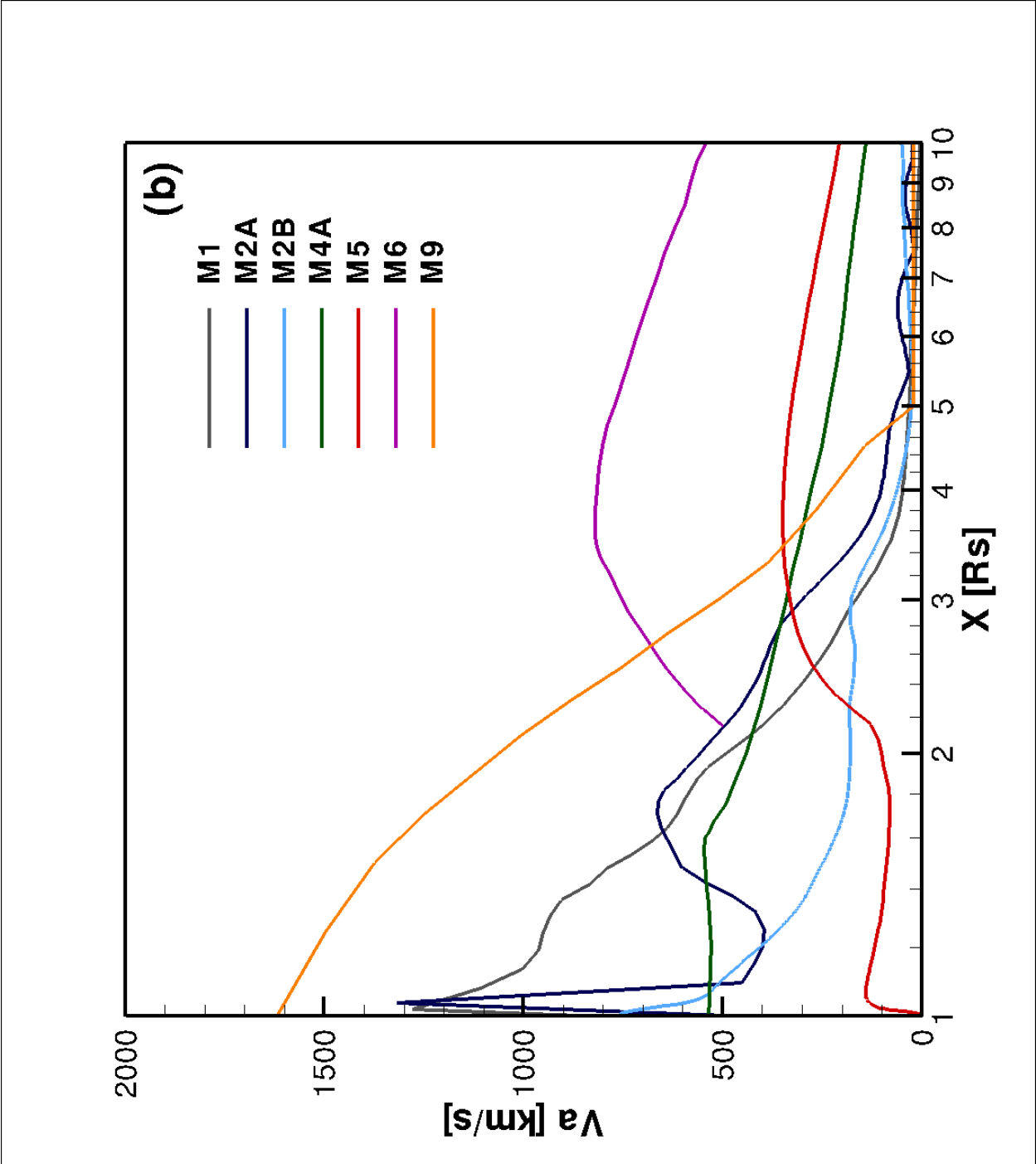
FIGURE 1: Alfvén speed profiles for (a) the polar open field regions, (b) streamers, and (c) active regions (c). The labels match with those in Table 1, and are given as follows: Manchester et al. 2004a, b (MA04; M1); Cohen et al. 2007 (CO07; M2); Roussev et al. 2004 (RO04; M3); Riley 2006 (RIL06; M4); Lionello, Linker & Mikic 2008 (LI08; M5); Guhathakurta, Sittler & Ofman 2006 (GSO06; M6); Mann et al. 2003 (MAN; M7); Cranmer, van Ballegoijen & Edgar 2007 (CR07; M8); Usmanov & Goldstein 2006 (UG06; M9); and Verdini & Velli 2007 (VE07; M10). For M4, the labels A-C correspond to the profiles with the following Carrington latitude and longitudes: A (0, 0) (quiet sun); B (10, 180) from the AR720; C (0, 180) below AR. For M2, the labels A-E correspond to: A and B are variations in thermal heating; C is straight out of AR8040; D and E are taken at an angle from the center of the AR, D is in the meridional plane and E in a plane parallel to the equatorial plane.

FIGURE 2: Color contour of Alfvén speed from model CO07. White lines indicate where the line cuts were taken for the poles and streamers.

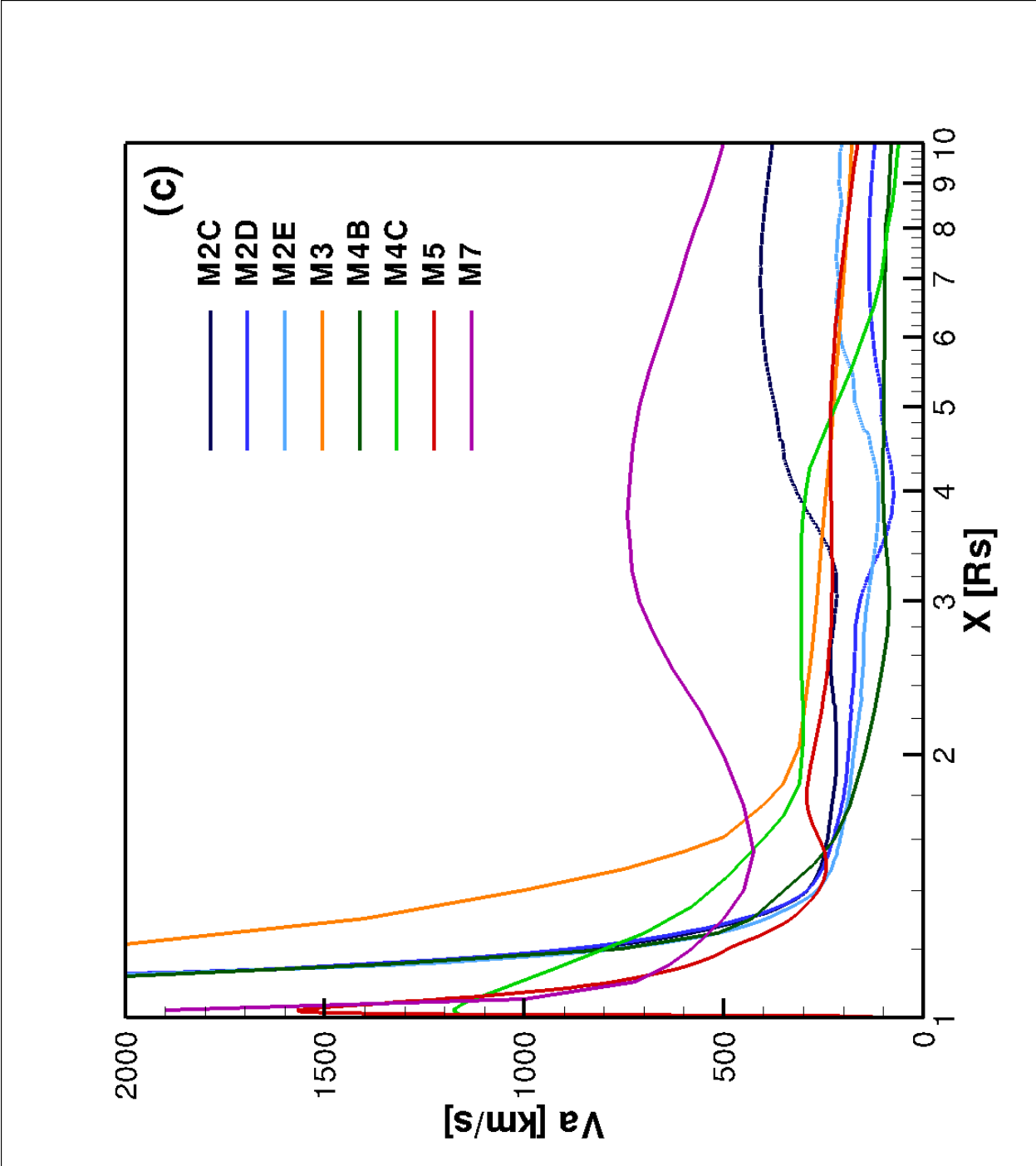
FIGURE 3: Alfvén speed for propagation in the meridional plane 0 degrees out of a streamer (solid lines) and 45 degrees away from the center of the streamer (dashed lines) (O. Cohen 2007 private communication). The labels a, b and c correspond to variations in thermal heating.



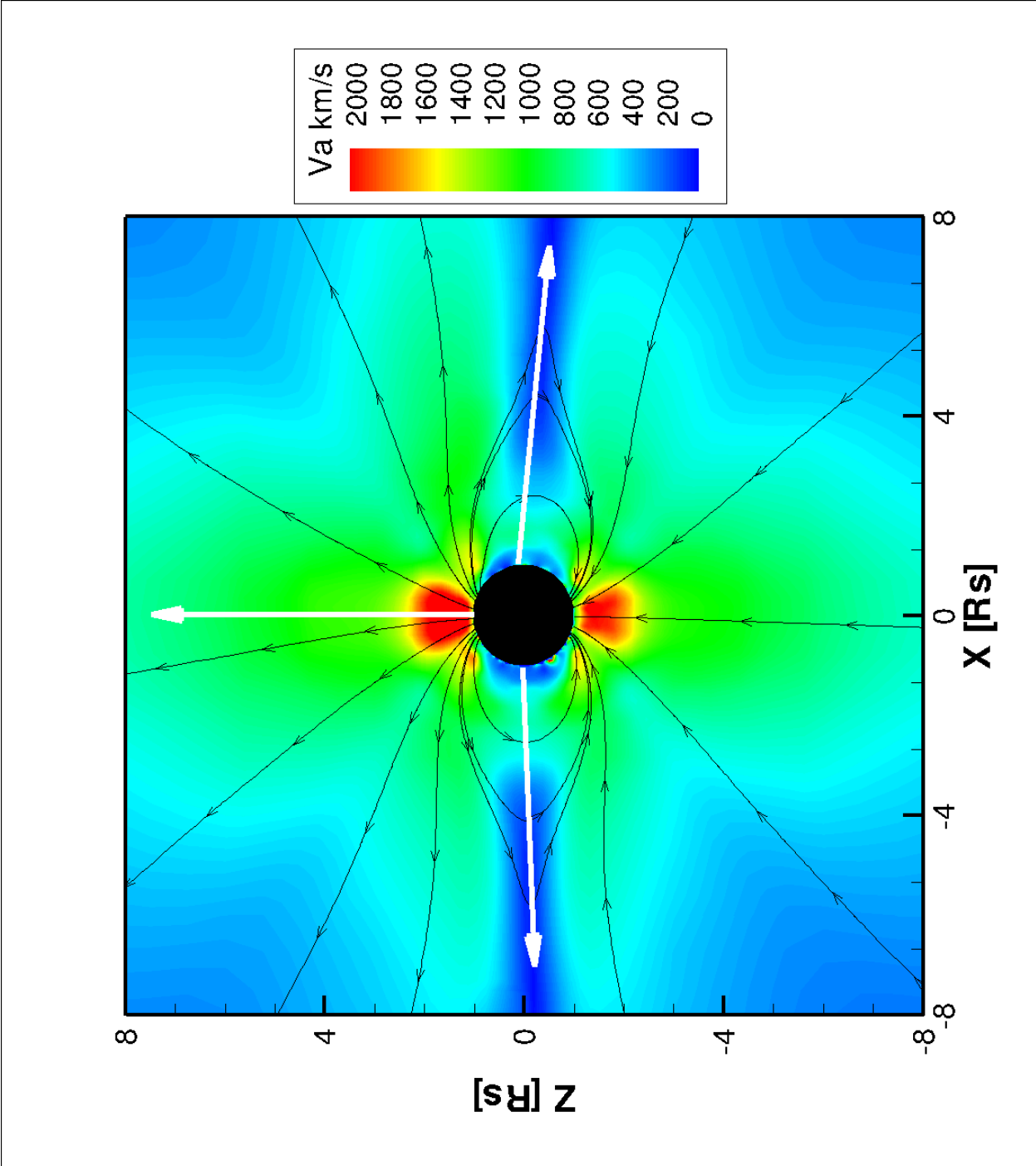
fla.eps



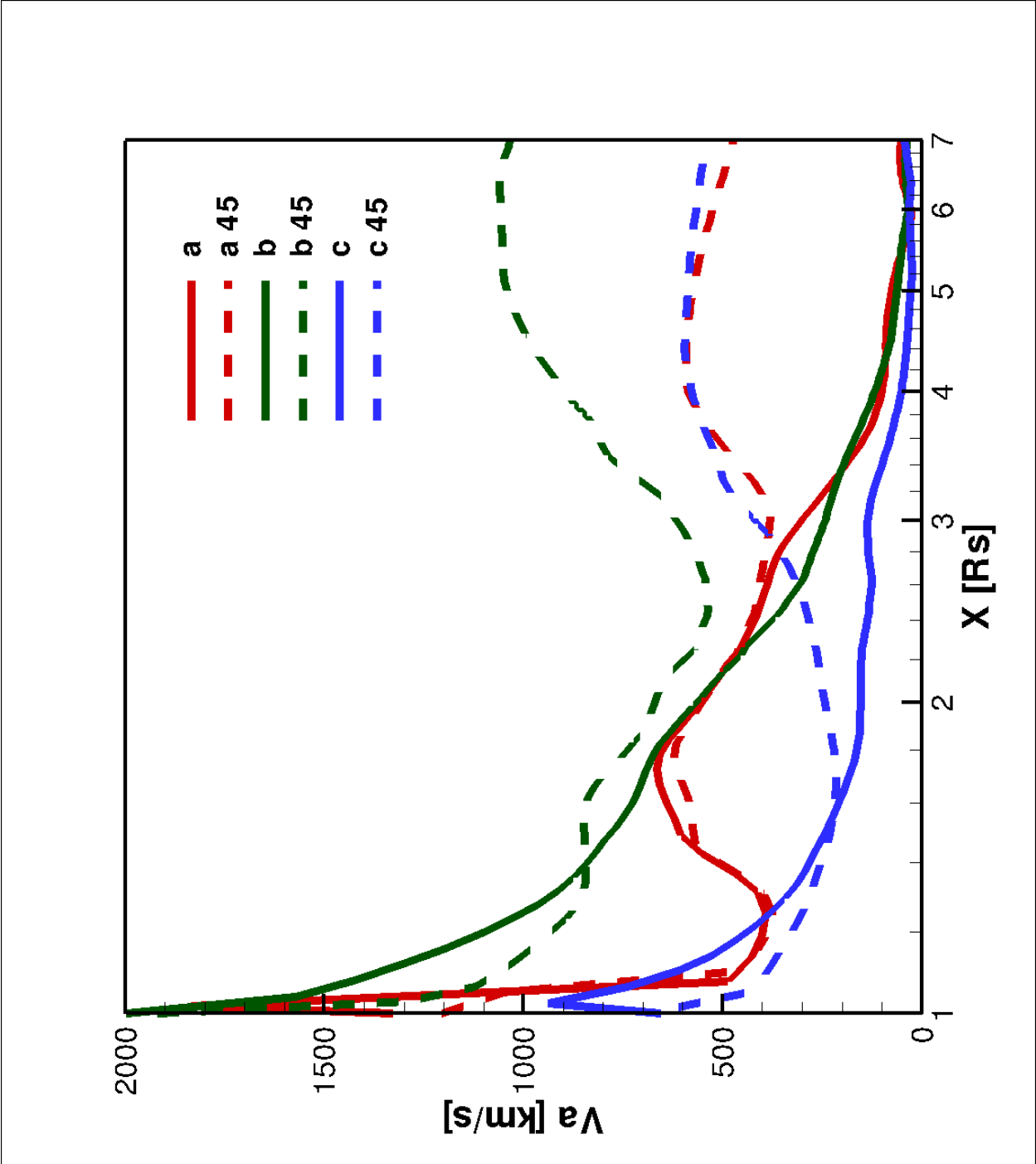
f1b.eps



flc.eps



f2.eps



f3.eps